J. Electrochem. Sci. Eng. **14(6)** (2024) 757-773; http://dx.doi.org/10.5599/jese.2329

Open Access : : ISSN 1847-9286
www.jESE-online.org

Original scientific paper

Fabrication of a molecularly imprinted poly(methyl methacrylate) decorated graphite electrode for detection of aloe-emodin in *Aloe vera*

Milan Dhara[1], Sanjoy Banerjee[2], Barnali Ghatak[3], Hemanta Naskar[4], Amit Kumar Chakraborty[5], Nityananda Das[6], Chezhiyan Kuppusamy[7], Gyan Prakash Sharma[7], Rajib Bandyopadhyay[8] and BipanTudu[8,✉]

[1]*Department of ECE, Future Institute of Engineering and Management, Kolkata, India*
[2]*Department of CSE (AI & ML), Future Institute of Technology, Kolkata, India*
[3]*Department of ECE, Aliah University, Kolkata, India*
[4]*IEM, University of Engineering and Management, Kolkata, India*
[5]*Department of Physics, NIT, Durgapur, India*
[6]*Department of Physics, JKC, Sidho-Kanho-Birsha University, Purulia, India*
[7]*National Food Laboratory, Kolkata, India*
[8]*Department of IEE, Jadavpur University, Kolkata, India*

Corresponding authors: ✉*bipantudu@gmail.com; Tel.: +91 23352587*

Received: March 20, 2024; Accepted: October 19, 2024; Published: October 26, 2024

Abstract

In this work, the authors represent a comprehensive approach for the development and validation of a novel graphite-supported molecularly imprinted poly(methyl methacrylate) electrode for the selective and sensitive detection of aloe-emodin (AE) in aloe-based cosmetic products. The electrocatalytic activity of the electrode was evaluated using cyclic voltammetry and differential pulse voltammetry techniques in phosphate buffer saline. Surface morphology, structural characteristics, and imprinting endorsement were investigated using field emission scanning electron microscopy, Fourier-transform infrared spectroscopy, and UV-Vis spectroscopy. Under the optimal conditions, the electrode showed an oxidative differential pulse voltammetry peak at -0.2931±0.011 V (vs. Ag/AgCl, saturated KCl). The current was increased linearly with increasing concentrations of AE from 0.0005 to 350 µM, with a low detection limit of 0.0003 µM. The voltammetric analysis has been validated by reverse-phase high-performance liquid chromatography (RP-HPLC) methods. A partial least square regression model was developed to correlate the results obtained from the proposed system with the reference values obtained by RP-HPLC. The model showed a high prediction accuracy of 95.95 % for the detection of AE in cosmetic samples. The developed electrode provides a low-cost, rapid, easy, and convenient method for the detection of AE in cosmetic products, offering potential benefits for quality control and safety assessment in the cosmetic industry.

Keywords
Aloe anthraquinone; molecular recognition; molecularly imprinted polymer; voltammetry; cosmetic products

Introduction

Anthraquinones are fundamental components found in naturally available herbs worldwide. They possess a variety of therapeutic properties, including antibacterial, diuretic, antiviral, laxative, and antitumor effects [1-4]. Aloe emodin (AE) is a specific type of aloe anthraquinone (1,8-dihydroxy-3-hydroxy-methyl-anthraquinone) found in plants of the Liliaceae family, such as *Aloe vera* (*Aloe barbadensis* Miller). It is known for its pharmaceutical, perfumery, flavour and fragrance, cosmetics, and aromatherapy applications [5]. It is intensively utilized in the tropic treatment of various skin complaints, especially wounds, irritations, frostbite, burns healing, and protection against skin damage from X-ray for its anti-inflammatory, antiseptic, antioxidant, and antibacterial properties [6-8]. AE finds widespread use in cosmetic products like moisturizers, sun creams, baby creams, wipes, bath aids, soaps, makeup, incense, shaving creams, and shampoo. Also, oral intake is used to treat constipation, ulcers, diabetes, cough, and headaches [9-11]. Moreover, several studies suggest that AE can produce genotoxicity, anti-tumour, regulation of immune function, promotion of appetite, and the effective prevention of AIDS [12,13]. Despite its beneficial effects, research on AE focuses on understanding its healing effects and potential toxicity. Regulation of its quantity in formulations and extracts remains an area of substantial research [14,15]. Therefore, it is very important to develop an efficient method to detect AE in a selective and sensitive way.

Various analytical methods, including high-performance liquid chromatography (HPLC) [16,17], gas chromatography/mass spectroscopy (GC-MS) [18], thin-layer chromatography (TLC) [19,20], and capillary electrophoresis mass spectrometry [21] have been studied to determine AE in *Aloe vera*. The main problem with these techniques is the high cost, time-consuming, and complex sample pretreatment. In contrast, the advancement of electrochemical sensors offers a precise and easy-to-handle alternative technique for quick and efficient quantitative detection of ingredients in cosmetic products [22]. These systems are described as user-friendly due to their simple operation, fast response times, low cost, simple sample preparation requirements, and customizable sensor-based sensitive and selective features. The technique critically analyses the reaction mechanism and dynamics parameters of analytes [23,24]. Diverse approaches were studied to enhance sensitivity, selectivity, and reproducibility in detecting various compounds, showcasing the innovation in analytical chemistry and sensor development. Dhara *et al*. [25] used this method to detect AE using platinum wire electrodes. Differential pulse polarography (DPP) was explored by Modi *et al.* [26] for quantitative analysis of AE in human blood and industrial samples. Li *et al.* [27] studied AE at carbon paste electrode, while screen-printed electrode using voltammetric technique for AE detection was investigated by Poosittisak *et al.* [28].

Surface modification is an alternative way to enhance the sensing potentials and detection limits of glassy carbon paste electrodes (CPE). Ionic liquids (ILs) enjoy inorganic anions and organic cations that act as binders and electron carriers for IL-modified CPE electrodes to enhance sensitivity. Wang *et al.* [29] used this approach to detect AE. Nickel nanoparticles modification was utilized by Bian *et al.* to increase the electrocatalytic activity of the glassy carbon electrode for AE detection [30]. Multi-wall carbon nanotube-modified glassy carbon electrode was developed by Yin *et al.* [31] for detecting emodin. Compared to carbon nanotubes, graphene has an excellent electrocatalytic activity for synthesizing biosensors due to its high gravimetric surface area and excellent carrier mobility. Li *et al.*

used graphene-Nafion-modified glassy carbon (GN-GC) electrodes for the sensitive detection of AE from natural extracts and urine samples [32]. In comparison to the above electrochemical methods, the molecularly imprinted polymer (MIP), an artificially synthesized receptor, was reported for sensitive detection of target molecules due to its high selective recognition property, stability, and reproducibility [33,34]. Wang *et al.* developed MIP through the electro-polymerization of pyrrole and AE to detect AE using electrochemical and colorimetric dual-mode sensing technology [35]. Hao *et al.* [36] further improved the previous work by using carbon nanoparticles (CNPs) as a modifier to improve the sensitivity of the sensor. In another way, El Gohary *et al.* [37] synthesized molecularly imprinted polymer-modified carbon paste electrodes to detect valaciclovir. Thermal polymerization technique was adopted by Motghare *et al*. [38] to develop an MIP-modified CPE electrode to detect uric acid in blood serum. Copper oxide nanoparticles were incorporated to further enhance the sensitivity and selectivity of MIP by Das *et al.* to detect gallic acid in green tea [39].

This work describes the fabrication and performance of a graphite-based molecularly imprinted poly(methyl methacrylate) (PMM-MIP@G) electrochemical sensor for the detection of AE. The sensor was fabricated by thermally polymerizing methyl methacrylate (MM) using AE as template molecules. Here, MM was selected as a functional monomer due to the strong physical interaction with graphite, which resulted in the formation of a rigid polymer structure with good conductivity [40]. The imprinted cavities on the MIP surface specifically adsorb only AE based on their predefined molecular recognition and chemical compatibility. In addition, the response of the sensor is validated using RP-HPLC to predict the content of AE in the real samples from different cosmetic brands, using a partial least squares regression (PLSR) based statistical algorithm.

Experimental

Chemicals and reagents

Aloe-emodin, methyl methacrylate, ethylene glycol dimethacrylate (EGDMA), sodium acetate trihydrate, sodium citrate dihydrate, benzoyl peroxide (BP), and graphite were purchased from Sigma-Aldrich. 1 mM of AE standard stock solution was prepared by directly dissolving 27 mg AE in 100 mL ethanol and then, other lower concentrations required for the experiment were achieved by simple dilution with ethanol. Sodium hydroxide (NaOH), ethanol and paraffin oil, used for the preparation of MIP, were purchased from Merck, India. Four different company aloe products (C1, C2, C3, and C4) were purchased from the local market. All reagents were of analytical grade unless otherwise specified. All required solutions needed for experiments were prepared by Millipore water received from the Merck Millipore system (resistance of about 18 MΩ). All experimental work was performed at normal room temperature (25 ± 2 °C).

Preparation of phosphate buffer solution

The preparation of phosphate buffer solution (PBS) of pH 6 was explained in our previous paper [41]. In brief, 0.63 g of oxalic acid ($C_2H_2O_4$) solution and 4 g of sodium hydroxide (NaOH) solution were prepared in 50 mL and 500 mL of Millipore water, respectively. Then, titration was performed thrice between 10 mL of oxalic acid and NaOH with phenolphthalein ($C_{20}H_{14}O_4$) as an indicator in order to standardize 0.1 M NaOH. Now, 112 mL of 0.1 M NaOH solution *is* mixed with 13.6 g of potassium dihydrogen phosphate (KH_2PO_4) in a volumetric flask. Millipore water was used to fill the 1 L level in the volumetric flask. The pH of the solution was adjusted using 0.1 M phosphoric acid (H_3PO_4) or 0.1 M NaOH. Acetate buffer solution (ABS) and citrate buffer solution (CBS) were prepared using sodium acetate trihydrate ($C_2H_9NaO_5$) and sodium citrate dehydrate ($C_6H_9Na_3O_9$), respectively.

Preparation of real samples

An amount of 0.35 g of each cosmetic product sample purchased from different producers (C1, C2, C3, and C4) was added to 100 mL of ethanol in a beaker and mixed in an ultrasonicator for 1 h. Then, the mixture was filtered by Whatman filter paper (particle retention of 11 µM) and stored in a volumetric flask for electrochemical detection of AE in cosmetic samples.

Synthesis of molecularly imprinted and non-imprinted poly(methyl methacrylate) material

Molecularly imprinted poly(methyl methacrylate) (MIP) materials were synthesized by in-situ polymerization of functional monomer, template, and cross-linker with a variable molar ratio as shown in Table 1. At first, 20 mL of ethanol in a beaker containing 0.90 g of commercial-grade graphite powder was put in an ultrasonicator for dispersion for 50 minutes. At the same time, MM and AE were mixed through ultrasonication in another beaker containing 30 mL of ethanol until a complex mixture of template molecules and functional monomer was developed *via* interfacial non-covalent bonding. Now, the as-prepared self-assembling monomer-template mixture was mixed with the dispersed graphite solution for 60 minutes through ultrasonication along with the addition of cross-linking agent EGDMA and BP (1 mg) as initiator. Finally, the entire mixture was transferred into a heater for thermal polymerization. The initial heater temperature was maintained at 60 °C and then the temperature was controlled to 30 °C. MIP-adduct was collected and dried overnight. For the preparation of MIP, as-prepared polymer material was washed with a mixture of ethanol and water (4:1 v/v) till the complete extraction of AE was confirmed and verified by FTIR spectra.

Different functional monomers, including acrylonitrile (AN), acrylic acid (AA), and N,N-dimethyl acrylamide (DMA) were used for the synthesis of MIPs, similar to the methods used for the PMM-MIP@G. Non-imprinted polymer (PMM-NIP@G) was synthesized using the same procedure without AE template molecules.

Table 1. *Materials synthesized and ratio of precursors used*

Polymer	Amount, mM			Molar ratio
	Template	Monomer	Cross linker	
PMM-MIP@G1	0.185	0.555	2.220	1:3:12
PMM-MIP@G2	0.185	0.740	3.700	1:4:20
PMM-MIP@G3	0.185	1.110	4.440	1:6:24
PMM-NIP@G	0.000	0.740	3.700	0:4:20

Fabrication of PMM-MIP@G, PMM-NIP@G and carbon paste electrodes

Firstly, 350 mg of the synthesized polymer material was ground properly in order to get a homogeneous fine powder. To get a fine paste, a few drops of paraffin oil were added as a binder. Subsequently, the prepared pastes were packed into fine capillary glass tubes (diameter = 0.25 cm, geometrical surface area = 0.0491 cm^2) and stuffed with a stainless-steel rod. For electrical contact with the electrodes, a copper wire was inserted into the backside of the tube. Other MIPs, including poly(acrylonitrile)-MIP (PAN-MIP@G), poly(acrylic acid)-MIP (PAA-MIP@G), poly(dimethyl acryl-amide)-MIP (PDMA-MIP@G), and non-imprinted polymer (PMM-NIP@G) electrode was prepared using the same procedure. For experimental compression, a bare CPE was prepared by hand mixing 350 mg of graphite powder and a few drops of paraffin oil with the help of agate mortar and pestle. The material was then packed into a capillary glass tube, similar to the method used for other electrodes.

Experiments and apparatus

Electrochemical measurements were carried out using computer-controlled Autolab PGSTAT 101 with software NOVA 1.11 from Metrohm Autolab, Netherlands. All electrochemical measurements were performed in a three-electrode cell containing a PMM-MIP@G working electrode, a platinum counter electrode, and a saturated Ag/AgCl/KCl_{sat} reference electrode. Characterization of all synthesized materials was performed by using field emission scanning electron microscopy (FESEM, JEOL-JEM-6700F), ultraviolet-visible (UV vis.) spectroscopy (Shimadzu UV-3600), and Fourier transform infrared spectroscopy from IR prestige 21, 200 VCE (FTIR, Shimadzu, Tokyo, Japan).

Results and discussion

Morphological investigation of PMM-MIP@G and PMM-NIP@G materials

The surface morphology of PMM-MIP@G (before and after wash) and PMM-NIP@G sensing materials were examined using FE-SEM, as shown in Figure 1(a-c). Figure 1(d) shows the surface morphology of NIP material that revealed a typical cross-linked network structure with a number of folds and crinkles corresponding to graphite, which enhanced the gravimetric surface area for loading imprinted polymer materials.

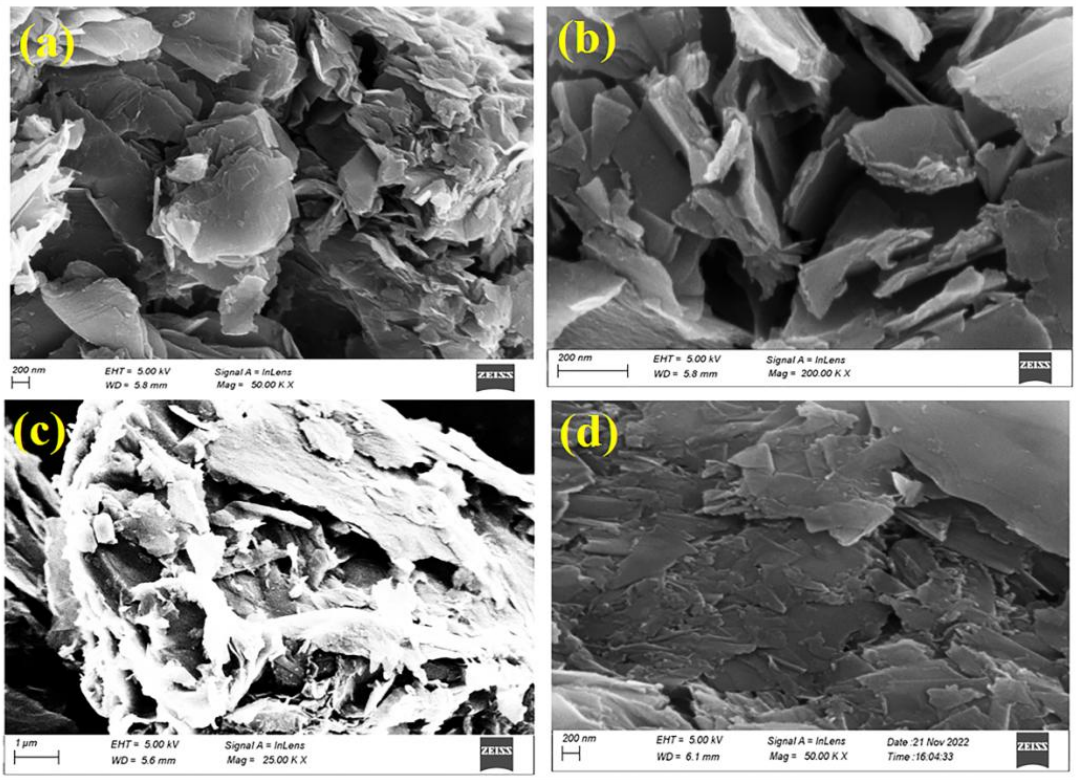

Figure 1. *FE-SEM images of: (a-b) PMM-MIP@G after wash, at different magnifications, (c) PMM-MIP adduct, and (d) NIP material*

After polymerization, a thin layer of imprinted polymer materials was uniformly incorporated into the graphite structure (Figure 1(c)). When the imprinted material was eluted with ethanol, a porous structure with large numbers of well-distributed cavities was observed (Figure 1(a-b)). The porous structure increases the electro-active area between active material and electrolyte, speeds up the ion diffusion of the electrolyte, and provides a better attachment platform for the electrochemically active sites, prompting a fast Faradaic reaction of AE molecules. The base layer of graphite provides a continuous electron transport path throughout the electrode region.

FTIR and UV-Vis analysis of PMM-MIP@G and PMM-NIP@G materials

FTIR spectroscopy was used to study the functional groups, chemical bonding, and composition of the synthesized polymers. Figure 2(a) shows the FTIR spectra of PMM-NIP@G and PMM-MIP@G before and after wash. In the MIP before and after extraction, the FTIR absorption peaks were observed at 3745 cm^{-1}, which is accredited to the stretching vibration of –OH. Peaks at 2962 cm^{-1} were attributed to the C-H asymmetric starching vibration of the alkyl chain [42]. The broadband peak cantered on 1742 cm^{-1} is caused by the stretching vibration of the carbonyl group (C=O) of monomer in the MIP. Peaks between 1550 to 1631 cm^{-1} correspond to different C-H bending vibrations belonging to CH_3 groups of MIP [43]. In the MIP adduct, bands near 1288 cm^{-1} are related to the stretching vibration of C-O, the peak near 1138 cm^{-1} is assigned to C-O-C asymmetric stretching, the peak near 933 cm^{-1} is attributed to O-CH_3 rocking, and the peak near 763 cm^{-1} indicates C-C stretching vibration of AE. In contrast, no peaks corresponding to AE molecules were observed for NIP and MIP after washing.

UV-Vis spectroscopy (λ = 200-800 nm) was used in order to study the interaction between polymerization components and the information on the successful templating of AE. Figure 2(b) shows that both the AE molecules and the PMM-MIP@G adduct have UV absorbance peaks at 282.3 nm, ascribed to the successful imprinting of AE within the synthesized polymer structure. However, no such absorbance peak was observed when AE was extracted from the MIP structure.

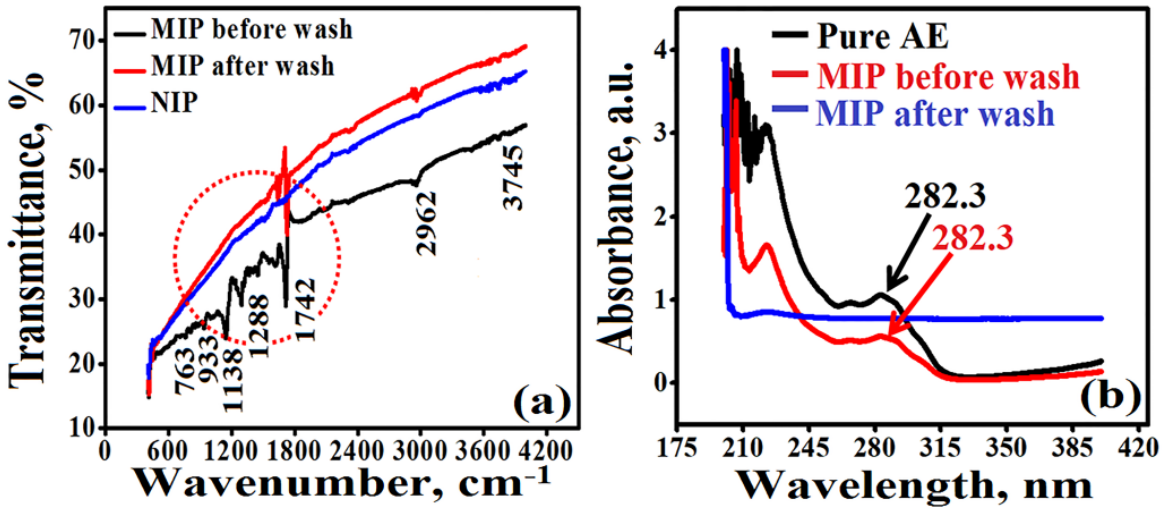

Figure 2. *(a) FTIR spectra of PMM-MIP@G before and after wash, and PMM-NIP@G, and (b) UV-vis spectra of pure AE, and MIP before and after washing*

Electrochemical behavior of AE at PMM-MIP@G electrode

Cyclic voltammetric (CV) measurements were carried out between -1.3 and 0.3 V *vs.* Ag/AgCl for the PMM-MIP@G electrode in 0.1 M PBS (pH 6.0) in the absence and presence of 100 µM AE. As shown in Figure 3(a), the PMM-MIP@G showed no response in the absence of AE, while the CV of AE exhibited a couple of well-defined redox peaks. The oxidation peak potential (E_{PA}) is at -0.117 V and the reduction peak potential (E_{PC}) at -0.713 V. The peak-to-peak potential separation (ΔE_P) is 0.596 V *vs*. Ag/AgCl, corresponding to a quasi-irreversible electron transfer process [44].

Further, the electrocatalytic behaviour of AE at PMM-MIP@G was compared with the responses at PMM-NIP@G and bare CPE, respectively (Figure 3(b)). The redox peak current (115.4 µA) obtained with the MIP sensor is 4.423 times higher than that with the NIP sensor. This is because MIP has more artificial recognition sites for the AE to be adsorbed during fabrication. At the same time, the bare CPE had no spikes.

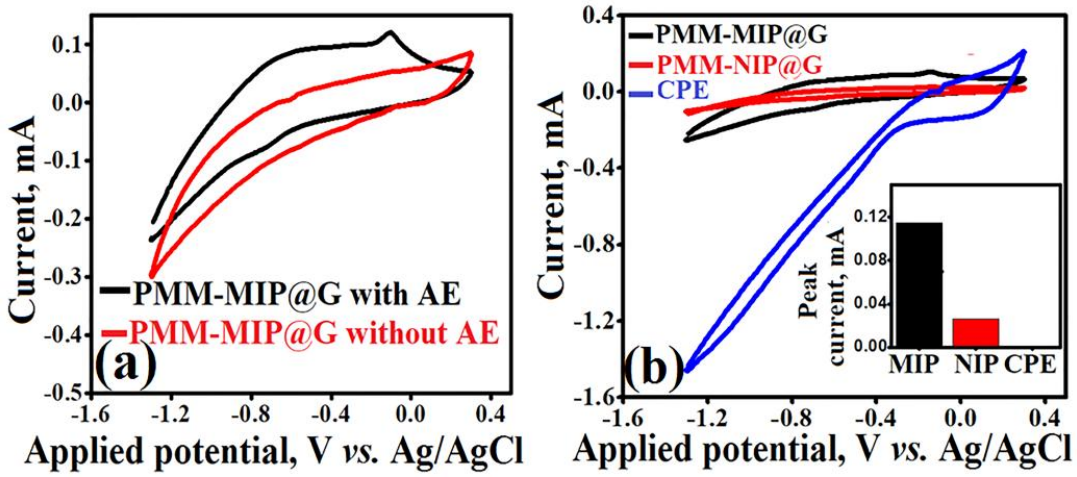

Figure 3. *CV of (a) 100 µM AE and without AE, and (b) 100 µM AE at PMM-MIP@G, PMM-NIP@G, and bare CPE sensors in 0.1 M PBS (pH 6.0) with a scan rate of 0.05 V s^{-1}. (Inset: bar plot of respective peak currents)*

Impact of monomer type and template-monomer molar ratio

The cyclic voltammogram response of PMM-MIP@G sensor was compared with that of PAN-MIP@G, PAA-MIP@G, and PDMA-MIP@G to select the appropriate monomer for detecting AE. PMM-MIP@G sensor showed the highest oxidation peak current of 115.4 µA, which is 4.6, 8.21, and 9.71 times greater than that of PAN-MIP@G, PAA-MIP@G, and PDMA-MIP@G, respectively as shown in Figure 4(a). Hence, MM was selected for further investigation.

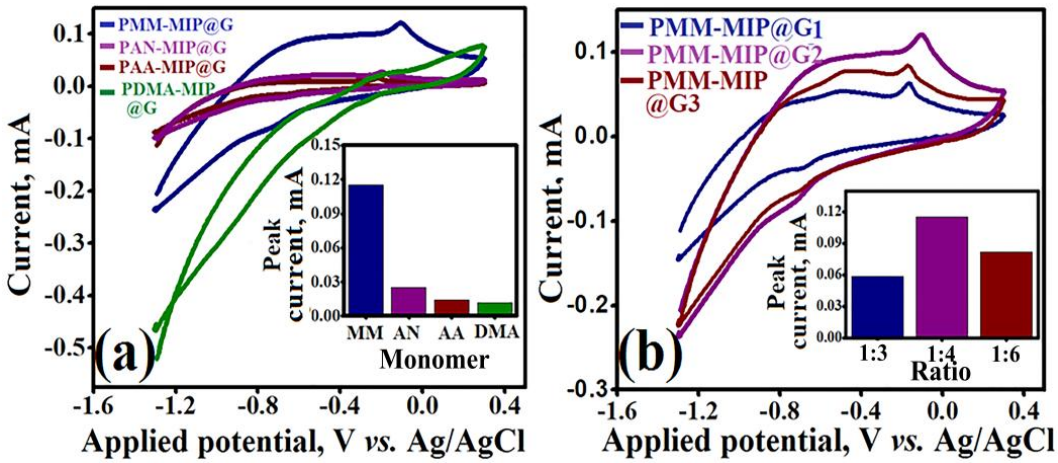

Figure 4. *CV of 100 µM AE in 0.1 M PBS (pH 6.0) with scan rate of 0.05 V s^{-1} at: (a) PMM-MIP@G, PAN-MIP@G, PAA-MIP@G, and PDMA-MIP@G sensor, and (b) PMM-MIP@G1, PMM-MIP@G2, and PMM-MIP@G3 sensor. (Inset: bar plot of their respective peak currents against different monomers and template-monomer ratio)*

In order to obtain optimum sensing material, different stoichiometric ratios of template, functional monomer, and cross-linker (Table 1) were studied. In cyclic voltammograms of AE, the PMM-MIP@G2 (molar ratio of 1:4:20) sensor yielded the highest anodic peak current (115.4 µA), which was 1.98 and 1.415 times higher than that of the PMM-MIP@G1 and PMM-MIP@G3, respectively as presented in Figure 4(b). This is mainly due to the favourable stoichiometric ratio of template, functional monomer, and cross-linker, yielding excellent uniform binding sites and thus increasing the selectivity of the developed sensor to AE. At a lower template-monomer ratio, AE molecules were probably not well captured, thus giving a lower response current of AE. Similarly, when a high template-monomer ratio was used, a small response of AE was attributed to the deep implanting of template molecules [45]. Hence, the molar ratio 1:4:20 was the optimal value for sensor fabrication.

Impact of supporting electrolyte and pH value

The influence of supporting electrolytes on the electrochemical responses of AE was studied using three different electrolytes, namely, phosphate buffer saline (PBS), acetate buffer saline (ABS), and citrate buffer saline (CBS). All electrolytes showed voltammograms with some difference in sensitivity and peak shape, as shown in Figure 5(a). The observation showed that the highest stable peak and voltammogram shape were achieved in the PBS buffer solution with peak currents 3.71 and 4.423 times higher than ABS and CBS buffer solutions, respectively. Hence, the PBS buffer solution was selected as the supporting electrolyte for further measurement.

The redox process of anthraquinone was frequently related to proton participation, which controls the reaction rate [46]. Hence, the influence of solution pH on the voltammetric sensing performance was studied using varying pH values of the solution, as shown in Figure 5(b). The adsorption response current of AE gradually increased with the increasing pH value from 2.0 to 6.0, and then, peak currents decreased slowly as the pH increased from 6.0 to 9.0. The peak potentials of the oxidative and reductive peaks were shifted to more negative values as pH was increased from 2.0 to 9.0, indicating that protons are involved in the electrochemical reaction. There are linear relationships between the peak potentials and pH as follows: E_{PA} = -0.0621 pH + 0.11 (R^2 = 0.96) and E_{PC} = -0.044 pH - 0.504 (R^2 = 0.92). The slopes were found to be equal to -62.1 and -44 mV/pH, which are close to the theoretical value of -59 mV/pH. This behaviour of AE confirms that the electron transfer is accompanied by an equal number of protons in the reaction. The number of protons (m) involved is 1.55 (≈2), obtained using the following equation: 0.059 $m/n\alpha$ =0.0621 (α = 0.737, n = 2) [47]. From this observation, pH 6.0 was chosen as the optimum condition for the supporting electrolyte.

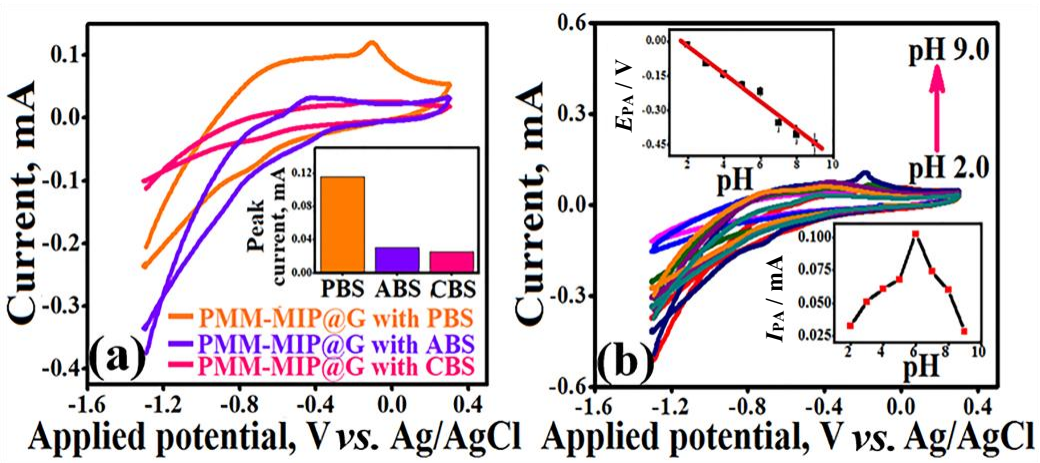

Figure 5. *CVs of PMM-MIP@G sensor at 100 µM AE: (a) in different buffer saline electrolytes (inset: bar plot of their peak currents), and (b) at different pH values of PBS (inset: plot of peak current vs. pH (below) and plot of peak potential vs. pH (above))*

Impact of scan rate using CV

The influence of the scan rate (v) on peak current and peak potential of AE (100 µM) was investigated by performing CV measurements to further characterize the interfacial kinetics and transport characteristics of the electrode. In the cyclic voltammograms of AE, the redox peak currents were gradually increased with the increase of v from 0.025 to 0.6 V s^{-1} (Figure 6(a)). The peak currents *vs*. scan rate were linear, what is represented in Figure 6(a) (inset), with linear regression equations as follows: I_{PA} = 0.425 ν + 0.039 (R^2 = 0.99) and I_{PC} = -0.204 ν - 0.027 (R^2 = 0.98). This confirms that AE at the electrode was primarily controlled by the surface adsorption quasi-reversible process. Also, a good linear relationship between the redox peak current and the square

root of scan rate (Figure 6(b), inset) was observed with corresponding regression equations as follows: I_{PA} = 0.40 $\nu^{½}$ - 0.0367 (R^2 = 0.98) and: I_{PC} = -0.193 $\nu^{½}$ + 0.0092 (R^2 = 0.98), indicating that the reaction process was also diffusion controlled. This diffusion-controlled characteristic was again cross-verified from the linear plot of the log of peak current *versus* the log of scan rate (Figure 6(b)) with the regression equation as log I = 0.661 log ν - 0.405 (R^2 = 0.99), having slope value of 0.661 which is close to 0.5 for the diffusion-controlled process [33,34].

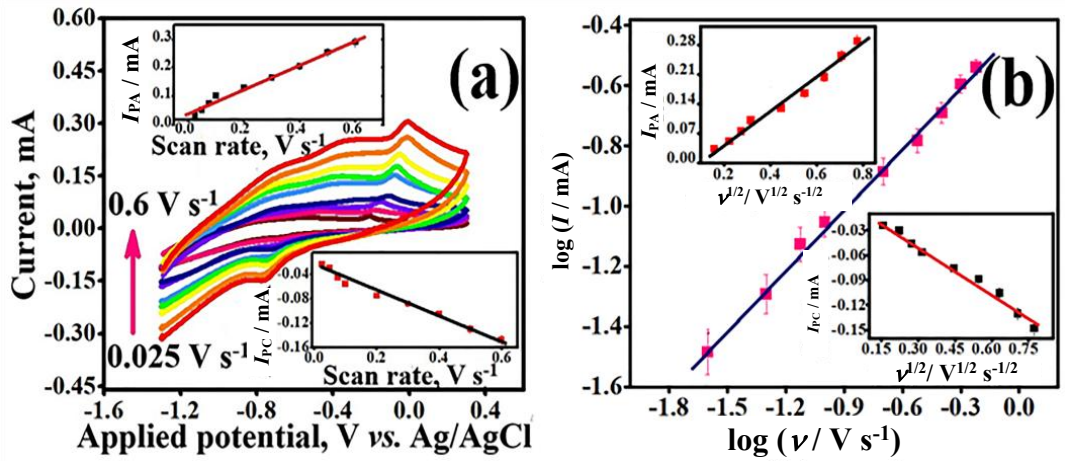

Figure 6. *(a) Effect of scan rate on CV of 100 μM AE in 0.1 M PBS (pH 6.0) using PMM-MIP@G sensor (inset: scan rate vs. oxidation peak current (above) and scan rate vs. reduction peak current (below), and (b) variation of log of peak current vs. log of scan rate (inset: square root of scan rate vs. anodic peak current (above) and square root of scan rate vs. cathodic peak current (below)*

The anodic peak potential (E_{PA}) was shifted positively, while the cathodic peak potential (E_{PC}) was shifted negatively with the increase in scan rate, indicating that the electrochemical reaction gradually became less reversible. The peak potentials and the logarithm of ν exhibited good linear relationships (Figure 7) with linear regression equations as follows: E_{PA} = 0.14 log ν - 0.0083 (R^2 = 0.96) and E_{PC} = -0.052 log ν - 0.747 (R^2 = 0.98). The slopes of the above expressions and Equations (1) and (2) were used to calculate the number of electrons transferred (n) and the anodic and cathodic charge transfer coefficients (α_a and α_c).

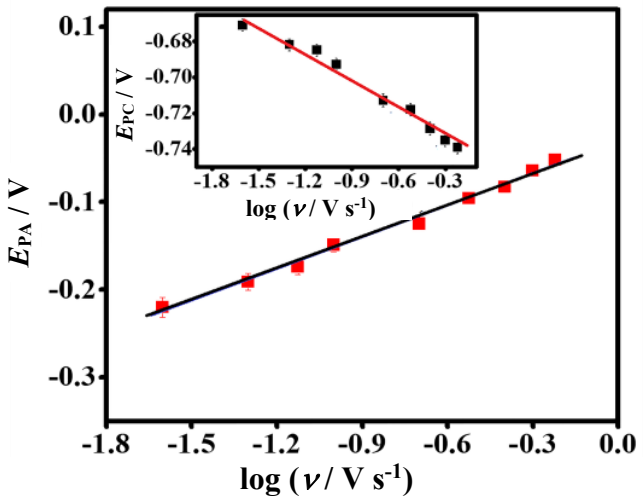

Figure 7. *Variation of anodic peak potential with log of scan rate (inset: cathodic peak potential vs. log of scan rate) at PMM-MIP@G sensor*

$$E_{PA} = a + \frac{2.303\,RT}{(1-\alpha_A)nF}\log \nu \qquad (1)$$

$$E_{PC} = b - \frac{2.303\,RT}{\alpha_C nF}\log\nu \quad (2)$$

Here, R represents the universal gas constant (8.314 J mol^{-1} K^{-1}), F symbolizes the Faraday constant (96500 C mol^{-1}), T / K denotes the absolute temperature, and a and b represent the constant. From Equation (1) and (2), the value of n was calculated to be 1.62 (≈2), indicating that AE at PMM-MIP@G involved two electron-transfer reactions. The calculated charge transfer coefficients α_a and α_c are 0.737 and 0.263, respectively. The deviation from the ideal value (0.5) indicates an asymmetrical relationship between the oxidized and reduced form of the compound.

Kinetic studies of PMM-MIP@G electrode

The average surface concentration (Γ) of AE on PMM-MIP@G electrode and the rate constant (k_s), which represents the electron transfer rate between AE molecules in the solution and at the tip of PMM-MIP@G electrode as estimated by Laviron equations (3) and (4) [33].

$$\log k_s = \alpha\log(1\text{-}\alpha) + (1\text{-}\alpha)\log\alpha - \log\frac{RT}{nF\nu} - \frac{\alpha(1\text{-}\alpha)nF\Delta E_p}{2.303\,RT} \quad (3)$$

$$I_p = \frac{n^2F^2A\Gamma\nu}{4RT} \quad (4)$$

In Equations (3) and (4), ΔE_p denotes potential difference, A represents the effective surface area of the electrode, and the other symbols have their usual meanings. From the slope of I_P *versus* v, the value of Γ was calculated to be 6.152×10^{-8} mol cm^{-2}. The larger surface area of the PMM-MIP@G electrode may facilitate more efficient entrapment of AE into the recognition sites within the composite polymer, thereby proving more active sites to participate in electron transfer [48]. The value of k_s was estimated to be 0.0235 s^{-1}.

Randles-Ševčik equation (5) was used to evaluate the surface area (A) of PMM-MIP@G and CPE electrode using the slope of I_P *vs.* $v^{1/2}$ linear plot in 5 mM of potassium ferrocyanide and PBS buffer solution. The electrochemically active surface areas of PMM-MIP@G and bare CPE were calculated to be 0.00282 and 0.001123 cm^2, respectively. This enhancement of the surface area of PMM-MIP@G leads to the sensitive response to AE.

$$I_P = 2.69\times10^5\, An^{3/2}D^{1/2}C\,\nu^{1/2} \quad (5)$$

Here, D signifies the diffusion coefficient (7.6×10^{-6} cm^2 s^{-1}), C symbolizes the concentration of analyte, and I_p represents the peak current.

Impact of concentration using differential pulse voltammetry

The effect of AE concentration on DPV peak currents was studied under the optimized experimental condition for AE at PMM-MIP@G due to the higher current sensitivity and resolution over CV as shown in Figure 8(a). The results showed that the peak current of AE at the PMM-MIP@G is linearly dependent on the AE concentration. The calibration plot was linear with two linear dynamic ranges as follows: 0.0005 to 1.0 µM (Figure 8(b) inset below) and 1 to 350 µM (Figure 8(b) inset above) with two linear regression equations as follows: $I_P = 16.92C_L + 6.004$ ($R^2 = 0.980$) and $I_P = 0.23C_U + 24.54$ ($R^2 = 0.99$) (C_L denotes lower concentrations of the first linear dynamic concentration range and C_U denotes higher concentrations of the second linear dynamic concentration range). The limit of detection (LOD) was evaluated from the calibration curve using the equation: LOD = 3s/m, where s is the standard deviation of the blank solution and m is the slope of the calibration curve in the low concentration range. The value of LOD was obtained as 0.0003 µM, which is lower than in previously reported articles, as shown in Table 2.

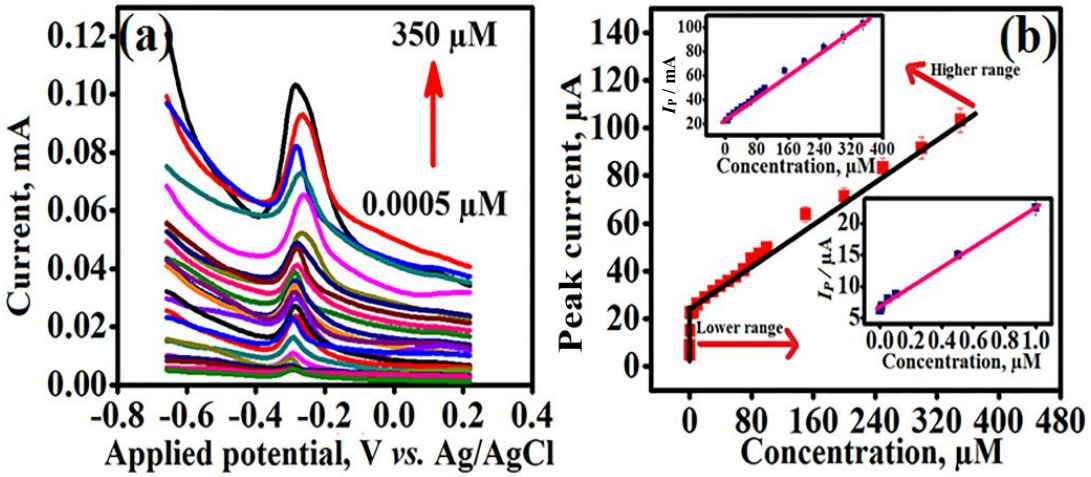

Figure 8. *DPV measurements of different AE concentrations in 0.1 M PBS (pH 6.0) using PMM-MIP@G sensor with pulse amplitude (ΔE_{Pulse}) of 50 mV, pulse width (t_{Pulse}) of 10 ms, scan rate (ν) of 0.05 V s^{-1}, and accumulation time (t_{acc}) of 60 s: (a) plot of current response against potential at varying AE concentrations, and (b) concentration vs. peak current plot (inset: plot of lower linear range (below) and higher linear range (above))*

Table 2. *Comparison of analytical results of the proposed method with literature results obtained by different voltammetry techniques*

Electrode	Technique	LOD, µM	Range of detection, µM	Ref.
MIP	adsorption isotherm	0.318	7.40-9251	[49]
MIP/Fe_3O_4/EGP	DPV	0.017	0.05-10	[35]
MWNT/GCE	CV	0.300	1.00- 100	[31]
CPIE	DPV	0.003	0.01 – 12.40	[29]
GN/GC	DPV	0.002	0.005 – 1.00	[32]
CNN/GCE	SWV	0.00208	0.00624 –1.13	[30]
PMM-MIP@G	DPV	0.00030	0.00050-350	This work

Selectivity and interference study

Influence of some organic and inorganic compounds that may coexist with the AE and AE-based cosmetic products, such as Mg^{2+}, Ca^{2+}, Na^{+}, Cu^{2+}, Zn^{2+}, K^{+}, SO_4^{2-} and Cl^{-} ions, were used to evaluate the specificity of the proposed electrode. The result indicated that 100-fold excess of these ions had no interference with the response of AE under optimized conditions (deviation below 5 % given in Table 3), as shown in Figure 9(a).

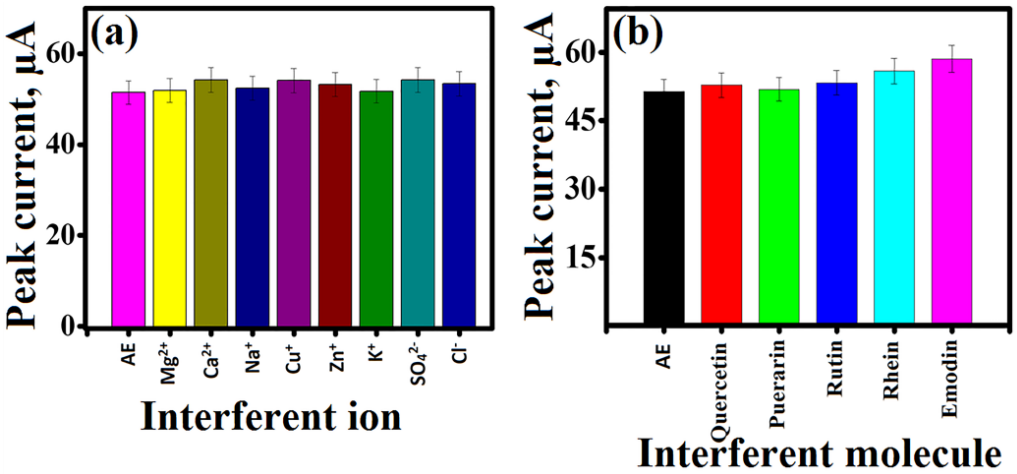

Figure 9. *Bar plot of variation of DPV peak current response of 100 µM AE in PBS buffer (pH 6.0) and (a) 10 mM of various interfering ions and (b) 100 µM of various interfering analog compounds*

Table 3. *Interference analysis of different species for determination of 100 µM AE at PMM-MIP@G sensor*

Interferent	Interferent concentration, mM	Peak current response with interferent, µA	RSD, %
Mg^{2+}	10.00	51.90	0.84
Ca^{2+}	10.00	54.20	4.43
Na^{+}	10 .00	52.40	-3.32
Cu^{2+}	10.00	54.10	3.34
Zn^{2+}	10.00	53.20	-1.67
K^{+}	10.00	51.70	-2.81
SO_4^{2-}	10.00	54.20	4.84
Cl^{-}	10.00	53.40	-1.48
Quercetin	0.10	52.81	2.60
Puerarin	0.10	51.92	0.87
Rutin	0.10	53.33	3.61
Rhein	0.10	55.86	8.53
Emodin	0.10	58.54	13.73

The selectivity of the PMM-MIP@G sensor was evaluated in the absence and presence of 100 µM of some interfering analog compounds, including quercetin, puerarin, rutin, emodin, and rhein having similar molecular structure and similar functional groups in a 100 µM solution of AE. The three DPV measurements of the mixed solution were taken for each of the interfering substances. The relative standard deviation (RSD) values were in the range of 0.87 to 3.61 % of the interfering substances quercetin, puerarin, and rutin and had no significant impact on the determination of AE. However, emodin and rhein interfering molecules increased the original sensing response (Figure 9(b)) by 13.73 and 8.53 %, respectively, due to their similar 9,10-anthraquinone structure that may be adsorbed onto the electrode surface.

Study of repeatability, reproducibility, and stability

Reproducibility, repeatability, and stability are the most important characteristics of any sensing device. Five successive DPV measurements (Figure 10(a) inset) of 100 µM of AE under optimum conditions using the same PMM-MIP@G sensor showed almost the same response with RSD of 2.14 %.

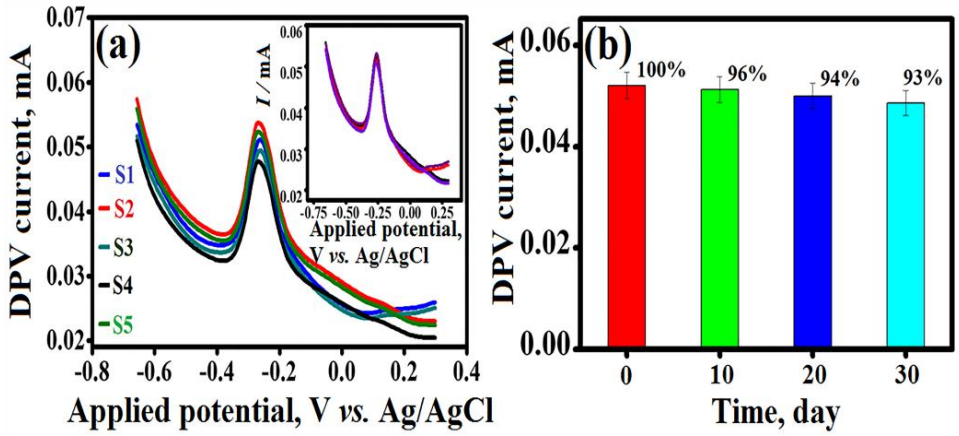

Figure 10. *DPV measurements of 100 µM AE in 0.1 M PBS (pH 6.0) using PMM-MIP@G sensor: (a) plot of current against potential for five different sensors (S1-S5), (inset: repeatability test for five measurements using the same sensor); (b) bar plot of DPV peak current of 100 µM AE against time interval (10-day) for stability test (the values over the bars shows changes of peak current value after 10 days interval, compared with the initial ones)*

Reproducibility was studied with five different PMM-MIP@G sensors prepared under the same condition independently with RSD of 5.71 %, as shown in Figure 10(a). Moreover, the peak current

of the fabricated PMM-MIP@G sensor was decreased to 93 % of the original value after 30 days of use (stored at room temperature), as shown in Figure 10(b). Hence, the sensor exhibited excellent reproducibility and remarkable long-term stability.

Electrochemical sensing of AE in cosmetic products

It was hypothesized above that the developed electrode could be employed in the analysis of cosmetic products to monitor the concentration level of AE. To validate this assumption, the electrochemical sensing response of the real sample was taken using a PMM-MIP@G electrode. The concentrations were determined at the PMM-MIP@G sensing electrode by taking fifteen repeated differential pulse voltammograms for each of the four cosmetic samples (C1, C2, C3, and C4). In order to validate the prediction performance of the developed electrode, a partial least square regression (PLSR) model was developed using DPV data and reference values obtained from RP-HPLC. MATLAB® Version 10 was used to execute the PLSR model. All real sample DPV data (615×15) were split into a training set (80 % of total data) and a test set (20 % of total data). During the onset of cross-validation, the training data set was formed by eliminating some data points, and the model was tested using that eliminating dataset. The prediction accuracy for all sample data was estimated using an iterative process. The highest prediction accuracy was obtained when the number of components of the developed model was selected to 8, as indicated by the root mean square error of cross-validation (RMSECV = 1.35) and correlation factor (CF = 0.984). The detection of AE exclusively in the C1 sample, at a concentration of 325.64 µM as measured by RP-HPLC, underscores its presence in that sample. Furthermore, the PLSR model predicted a concentration of 312.46 µM of AE in the C1 sample, showcasing a remarkable average prediction accuracy of 95.95 % when compared to the RP-HPLC results. However, it is important to note that the absence of AE in the C2, C3, and C4 samples does not definitively indicate that AE is absent. Potential reasons for non-detection of AE using the developed sensor with regression model may include instability and eventual degradation of AE in these real samples under certain conditions. For instance, photodegradation may cause the breakdown of AE, heat sensitivity may cause chemical changes in the structure of the compound, pH instability in extremely acidic or basic conditions leads to hydrolysis or other chemical reactions, oxidative degradation of AE results in the formation of inactive by-products, and solvent compatibility. Understanding these factors that contribute to the instability and degradation of AE is crucial for the detection of AE in these real samples.

Conclusion

In summary, a novel approach for rapid, sensitive, and highly selective voltammetric detection of AE was proposed. This method involved the incorporated molecularly imprinted poly(methyl methacrylate) (MIP) with a graphite-supported sensitive electrode, enabling sensitive and selective detection of AE in aloe-based cosmetic samples from various brands (C1, C2, C3, and C4) in a simple and inexpensive manner. The developed sensing electrode showed excellent stability and outstanding reproducibility, along with the interference immune response, ensuring reliable and consistent results. The sensing electrode exhibited two linear dynamic ranges, covering concentrations ranges from 0.0005 to 1.0 µM and 1.0 to 350 µM, with a low limit of detection of 0.0003 µM. A partial least squares (PLSR) model was developed to correlate the sensing results with reference values obtained from RP-HPLC, achieving a high prediction accuracy of approximately 95.95 %. The developed sensor shows promising result in terms of LOD, what highlights its superior sensitivity compared to existing methods. Hence, this work represents a significant advancement in electrochemical sensing,

offering a reliable and efficient platform for detecting AE, particularly in aloe-based cosmetic products.

***Acknowledgements**: The authors have acknowledged to the Department of Physics, National Institute of Technology, Durgapur for the FE-SEM, and FTIR facilities.*

References

[1] A. Shedoeva, D. Leavesley, Z. Upton, C. Fan, Wound healing and the use of medicinal plants, *Evidence-Based Complementary and Alternative Medicine* **2019** (2019) 2684108. https://doi.org/10.1155/2019/2684108

[2] S.S. Pammi, B. Suresh, A. Giri, Antioxidant potential of medicinal plant*, Journal of Crop Science and Biotechnology* **26** (2023) 13-26. https://doi.org/10.1007/s12892-022-00159-z

[3] J. Kolodziejczyk-Czepas, O. Liudvytska, *Rheum rhaponticum* and *Rheum rhabarbarum*: A review of phytochemistry, biological activities and therapeutic potential*, Phytochemistry Reviews* **20** (2021) 589-607. https://doi.org/10.1007/s11101-020-09715-3

[4] S. Siddamurthi, G. Gutti, S. Jana, A. Kumar, S.K. Singh, Anthraquinone: a promising scaffold for the discovery and development of therapeutic agents in cancer therapy, *Future Medicinal Chemistry* **12** (2020) 1037-1069. https://doi.org/10.4155/fmc-2019-0198

[5] A.S. Jadhav, O. A. Patil, S.V. Kadam, M.A. Bhutkar, Review on *Aloe Vera* is used in medicinal plant*, Asian Journal of Research in Pharmaceutical Science* **10** (2020) 26-30. https://doi.org/10.5958/2231-5659.2020.00006.5

[6] C. Egbuna, E. Gupta, S.M. Ezzat, J. Jeevanandam, N. Mishra, M. Akram, N. Sudharani, C.O. Adetunji, P. Singh, J.C. Ifemeje, M. Deepak, A. Bhavana, A.M.P. Wang, R. Ansari, J. B. Adetunji, U. Laila, M.C. Olisah, P.F. Onyekere, *Aloe species as valuable sources of functional bioactives*. in: C. Egbana, G.D. Tupas (Eds), *Functional Foods and Nutraceuticals, Bioactive Components, Formulations and Innovations,* Springer Nature, Switzerland*,* 2020, 337-387. https://doi.org/10.1007/978-3-030-42319-3_18

[7] C. Altinkaynak, E. Haciosmanoglu, M. Ekremoglu, M. Hacioglu, N. Özdemir, Anti-microbial, anti-oxidant and wound healing capabilities of *Aloe vera*-incorporated hybrid nanoflowers, *Journal of Bioscience and Bioengineering* **135** (2023) 321-330. https://doi.org/10.1016/j.jbiosc.2023.01.004

[8] P.K. Sahu, D.D. Giri, R. Singh, P. Pandey, S. Gupta, A.K. Shrivastava, A. Kumar, K.D. Pandey, Therapeutic and medicinal uses of *Aloe vera*: a review, *Pharmacology & Pharmacy* **4** (2013) 599. http://dx.doi.org/10.4236/pp.2013.48086

[9] N.M.S. Selvaraja, Z. Edis, N.I.W. Azelee, Facile Synthesis of Antimicrobial Aloe Vera for Cosmetic Application, *Bioprocessing and Biomass Technology* **1** (2022) 39-47. https://doi.org/10.11113/bioprocessing.v1n1.15

[10] M.M. Rahman, R. Amin, T. Afroz, J. Das, Pharmaceutical, Therapeutically and Nutraceutical Potential of Aloe Vera: A Mini-Review, *Journal of Pharmaceutical Research International* **33** (2021) 109-118. https://doi.org/10.9734/JPRI/2021/v33i37A31986

[11] Y. Gao, K.I. Kuok, Y. Jin, R. Wang, Biomedical applications of *Aloe vera*, *Critical Reviews in Food Science and Nutrition* **59** (2019) S244-S256. https://doi.org/10.1080/10408398.2018.1496320

[12] M.H. Radha, N.P. Laxmipriya, Evaluation of biological properties and clinical effectiveness of *Aloe vera*: A systematic review, *Journal of Traditional and Complementary Medicine* **5** (2015) 21-26. https://doi.org/10.1016/j.jtcme.2014.10.006

[13] M. Tiwari, M. Upadhayay, The medicinal plant components and applications (Aloe vera), *Journal of Medicinal Plants Studies* **6** (2018) 89-95. https://www.plantsjournal.com/archives/2018/vol6issue3/PartB/6-3-27-633.pdf

[14] X. Dong, Y. Zeng, Y. Liu, L. You, X. Yin, J. Fu, J. Ni, Aloe-emodin: a review of its pharmacology, toxicity, and pharmacokinetics, *Phytotherapy Research* **34** (2020) 270-281. https://doi.org/10.1002/ptr.6532

[15] X. Guo, N. Mei, *Aloe vera*: A review of toxicity and adverse clinical effects*, Journal of Environmental Science and Health*, *Part C* **34** (2016) 77-96. https://doi.org/10.1080/10590501.2016.1166826

[16] S. Tabin, R.C. Gupta, G. Bansal, A.N. Kamili, Comparative HPLC analysis of emodin, aloe emodin and rhein in *Rheum emodi* of wild and in vitro raised plants, *Journal of Pharmacognosy and Phytochemistry* **5** (2016) 121-130. https://www.phytojournal.com/archives/2016/vol5issue2/PartB/5-1-50.pdf

[17] V. Jain, L. Tandel, R. Sonone, Novel isocratic RP-HPLC method for simultaneous estimation of Berberine and Aloe-emodin, *Research Journal of Pharmacy and Technology* **14** (2021) 657-661. http://dx.doi.org/10.5958/0974-360X.2021.00117.7

[18] M.A. ElSohly, W. Gul, T.P. Murphy, Analysis of the anthraquinones aloe-emodin and aloin by gas chromatography/mass spectrometry, *International Immunopharmacology* **4** (2004) 1739-1744. https://doi.org/10.1016/j.intimp.2004.07.005

[19] A. Sihanat, C. Palanuvej, N. Ruangrunsi, K. Rungsihirunrat, Estimation of aloe-emodin content in Cassia grandis and Cassia garrettiana leaves using TLC densitometric method and TLC image analysis, *Indian Journal of Pharmaceutical Sciences* **80** (2018) 359-365. http://dx.doi.org/10.4172/pharmaceutical-sciences.1000365

[20] S. Narayanan, A.P. Jadhav, Simultaneous estimation of aloe emodin and emodin *from Rheum emodi*, *Cassia alata* and *Aloes* by HPTLC, *Indian Journal of Pharmaceutical Sciences* **77** (2015) 783-787. https://doi.org/10.4103/0250-474x.174994

[21] J. Cheng, L. Wang, W. Liu, D.D. Chen, Quantitative Nonaqueous Capillary Electrophoresis–Mass Spectrometry Method for Determining Active Ingredients in Plant Extracts, *Analytical Chemistry* **89** (2017) 1411-1415. https://doi.org/10.1021/acs.analchem.6b04944

[22] T. Dodevska, D. Hadzhiev, I. Shterev, Electrochemical sensors for the safety and quality control of cosmetics: An overview of achievements and challenges, *Journal of Electrochemical Science and Engineering* **14** (2024) 3-35. https://doi.org/10.5599/jese.1507

[23] J.G. Manjunatha, Surfactant modified carbon nanotube paste electrode for the sensitive determination of mitoxantrone anticancer drug*, Journal of Electrochemical Science and Engineering* **7** (2017) 39-49. https://doi.org/10.5599/jese.368

[24] S.Z. Mohammadi, F. Mousazadeh, A sensitive sensor based on graphitic carbon nitride/1-butyl-3-methylimidazolium hexafluorophosphate ionic liquids modified carbon paste electrode for sensing of carmoisine dye in food samples, *Journal of Electrochemical Science and Engineering* **12** (2022) 1143-1152. https://doi.org/10.5599/jese.1396

[25] M. Dhara, S. Banerjee, H. Naskar, B. Ghatak, S.K. Babar Ali, N. Das, R. Bandyopadhyay, B. Tudu, Electrochemical Detection of Aloe Emodin using Platinum Electrode Based Voltammetry Technique, *Journal of Material Sciences & Manufacturing Research* **146** (2023) 1-6. https://doi.org/10.47363/JMSMR/2023(4)146

[26] G. Modi, K.S. Pitre, Significance of Species Sensitive Electrochemical Methods for the Analysis of Antineuractodermal Agent AE (Aloe-Emodin), *Reviews in Analytical Chemistry* **29** (2010) 117-128. https://doi.org/10.1515/REVAC.2010.29.2.117

[27] J. N. Li, P. Gao, X. Li, Z. Yan, X. Mao, Study on the adsorptive catalytic voltammetry of aloe-emodin at a carbon paste electrode, *Science in China Series B: Chemistry* **48** (2005) 442-448. https://doi.org/10.1360/042004-33

[28] S. Poosittisak, P. Wongkaew, Electrochemical study of aloe gel and emodin on a screen printed carbon electrode, *International Journal of GEOMATE* **11** (2016) 2815-2819. http://dx.doi.org/10.21660/2016.28.1477

[29] Y. Wang, *H. Xiong, X. Zhang, S. Wang,* Electrochemical study of Aloe-emodin on an ionic liquid-type carbon paste electrode, *Microchimica Acta* **169** (2010) 255-260 http://dx.doi.org/10.1007/s00604-010-0348-7

[30] C. Bian, L. Zhang, H. Xiong, X. Zhang, S. Wang, Electrochemical behavior of herbal antitumor drug aloe emodin at carbon coated nickel magnetic nanoparticles modified glassy carbon electrode, *Electroanalysis* **22** (2010) 2658-2664. https://doi.org/10.1002/elan.201000211

[31] Z. H. Yin, Q. Xu, Y. Tu, Q. J. Zou, J. H. Yu, Y. D. Zhao, *Bioelectrochemistry* **72** (2008) 155-160. https://doi.org/10.1016/j.bioelechem.2008.01.005

[32] J. Li, J. Chen, X.-L. Zhang, C. H. Lu, H. H. Yang, A novel sensitive detection platform for antitumor herbal drug aloe-emodin based on the graphene modified electrode, *Talanta* **83** (2010) 553-558. https://doi.org/10.1016/j.talanta.2010.09.058

[33] A. Gómez-Caballero, N. Unceta, M.A. Goicolea, R.J. Barrio, Voltammetric determination of metamitron with an electrogenerated molecularly imprinted polymer microsensor, *Electroanalysis* **19** (2007) 356-363. https://doi.org/10.1002/elan.200603731

[34] H. Wang, H. Zhao, X. Quan, S. Chen, Electrochemical determination of tetracycline using molecularly imprinted polymer modified carbon nanotube-gold nanoparticles electrode, *Electroanalysis* **23** (2011) 1863-1869. https://doi.org/10.1002/elan.201100049

[35] M. Wang, X. Kan, Imprinted polymer/Fe_3O_4 micro-particles decorated multi-layer graphite paper: Electrochemical and colorimetric dual-modal sensing interface for aloe-emodin assay, *Sensors and Actuators B: Chemical* **323** (2020) 128672. https://doi.org/10.1016/j.snb.2020.128672

[36] Q. Hao, L. Lu, X. Kan, Probe and analogue: double roles of thionine for aloe-emodin selective and sensitive ratiometric detection, *Sensors and Actuators B: Chemical* **292** (2019) 247-253. https://doi.org/10.1016/j.snb.2019.04.129

[37] N.A. El Gohary, A. Madbouly, R.M. El Nashar, B. Mizaikoff, Voltammetric determination of valaciclovir using a molecularly imprinted polymer modified carbon paste electrode, *Electroanalysis* **29** (2017) 1388-1399. https://doi.org/10.1002/elan.201600784

[38] R.V. Motghare, K.K. Tadi, P. Dhawale, S. Deotare, A.K. Kawadkar, R. Chillawar, S. Khan, Voltammetric determination of uric acid based on molecularly imprinted polymer modified carbon paste electrode, *Electroanalysis* **27** (2015) 825-832. https://doi.org/10.1002/elan.201400579

[39] D. Das, D. Biswas, A.K. Hazarika, S. Sabhapondit, R.B. Roy, B. Tudu, R. Bandyopadhyay, CuO nanoparticles decorated MIP-based electrode for sensitive determination of gallic acid in green tea, *IEEE Sensors Journal* **21** (2020) 5687-5694. https://doi.org/10.1109/JSEN.2020.3036663

[40] L. Zhang, J. Zhu, W. Zhou, J. Wang, Y. Wang, Thermal and electrical conductivity enhancement of graphite nanoplatelets on form-stable polyethylene glycol/polymethyl methacrylate composite phase change materials, *Energy* **39** (2012) 294-302. https://doi.org/10.1016/j.energy.2012.01.011

[41] S. Banerjee, M. Dhara, H. Naskar, B. Ghatak, S.B. Ali, N. Das, D.K. Das, R. Bandyopadhyay, B. Tudu, Selective Electrochemical Detection of Thymoquinone in Black Cumin Using Titanium Oxide-Modified Graphite Paste Electrode, *Nano LIFE* **14** (2024) 2450001. https://doi.org/10.1142/S1793984424500016

[42] V.N.K.S.K. Nersu, B.R. Annepu, S.S. Rajaputra, S.S.B. Patcha, Char of Tagetes erecta (African marigold) flower as a potential electrode material for supercapacitors, *Journal of Electrochemical Science and Engineering* **12** (2022) 787-797. http://dx.doi.org/10.5599/jese.1381

[43] H. Verma, R.K. Pandey, S.S. Shukla, B. Gidwani, A. Vyas, Investigation of Effect of Phytoconstituents Aloe Emodin and Quercetin on Bioavailability of Albendazole, *Indian*

Journal of Pharmaceutical Education and Research **54** (2020) 991-998. https://doi.org/10.5530/ijper.54.4.193

[44] H. Tashakkorian, B. Aflatoonian, P.M. Jahani, M.R. Aflatoonian, Electrochemical sensor for determination of hydroxylamine using functionalized Fe_3O_4 nanoparticles and graphene oxide modified screen-printed electrode, *Journal of Electrochemical Science and Engineering* **12** (2022) 71-79. http://dx.doi.org/10.5599/jese.1145

[45] K.F. Pratama, M.E.R. Manik, D. Rahayu, A.N. Hasanah, Effect of the molecularly imprinted polymer component ratio on analytical performance, *Chemical and Pharmaceutical Bulletin* **68** (2020) 1013-1024. https://doi.org/10.1248/cpb.c20-00551

[46] P.S. Guin, S. Das, P.C. Mandal, Electrochemical reduction of quinones in different media: a review, *International Journal of Electrochemistry* **2011** (2011) 816202. https://doi.org/10.4061/2011/816202

[47] E. Arslan, S. Çakır, Electrochemical fabrication of polyproline modified graphite electrode decorated with Pd–Au bimetallic nanoparticles: Application for determination of carminic acid, *Journal of Electroanalytical Chemistry* **760** (2016) 32-41. https://doi.org/10.1016/j.jelechem.2015.11.042

[48] A.E. Vikraman, D. Thomas, S.T. Cyriac, K.G. Kumar, Kinetic and thermodynamic approach in the development of a voltammetric sensor for sunset yellow, *Journal of The Electrochemical Society* **161** (2014) B305. https://iopscience.iop.org/article/10.1149/2.0581414jes/meta

[49] M. L. Tian, Y. R. Lee, D. W. Park, K. H. Row, Selective solid-phase extraction of aloe emodin from aloe by molecularly imprinted polymers, *Chemical Research in Chinese Universities* **29** (2013) 663-666. https://doi.org/10.1007/s40242-013-2357-7